

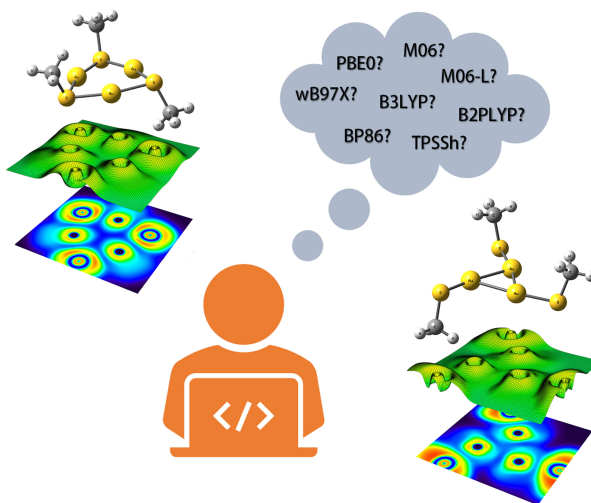
Small Gold-Thiolate Clusters $\text{Au}_3(\text{SMe})_3$: Benchmarking of Density Functionals and Bonding Analysis

Maya Khatun, Sayan Paul, Saikat Roy, Subhasis Dey, and Anakuthil Anoop*

*Department of Chemistry, Indian Institute of Technology Kharagpur, Kharagpur 721302,
India*

E-mail: anoop@chem.iitkgp.ac.in

Abstract



We present a benchmark study on popular density functionals for their efficiency and accuracy in the geometry and relative stability of gold-thiolate nanoclusters taking $\text{Au}_3(\text{SMe})_3$ isomers. We have used normalized mean absolute error (NMAE) analysis as a parameter to compare the results with the reference methods – DLPNO-CCSD(T)

and RI-SCS-MP2. We have also compared the performance on the thiolate interaction energy of the stable geometries using the results from our benchmark study. One of the promising functionals is PBE that shows robust performance for geometry optimization. On the other hand, M06-2X stands out as the proper choice for the relative energies of the clusters. With the selected methods, we have analyzed the gold-sulfur interaction in $\text{Au}_3(\text{SMe})_3$ and a comparison is made with AuSMe. The bonding analysis has revealed a partial covalency between gold and sulfur atoms in general. On going from AuSMe to $\text{Au}_3(\text{SMe})_3$, a substantial flow of charge from gold atoms to thiolate ligands as a result of the increase in gold *s-d* hybridization. As the *s-d* mixing in Au increases, the main character of Au-S interaction shifts from covalent to ionic. Hence, a covalent-charge-transfer interaction dominates in gold-sulfur bonding and gives rise to a charge-shift bonding.

Introduction

Interaction between gold clusters and thiolates has gathered significant interest in the scientific world for several decades. Thiolate-protected gold nanoclusters have plentiful applications in medicine,¹ catalysis,² and sensing.³ Gold systems in atomic scale and bulk metallic scale have distinct properties. Gold nanoparticles bigger than ~ 2 nm have a face-centered cubic (fcc) structure, and their optical properties show metallic nanocrystal nature by the surface plasmon resonance activity.⁴ In particular, quantization of electronic energy is observed as the cluster size decreases due to quantum confinement effects. The energy band in small-scale nanoclusters gets separated into discrete energy levels like the molecular energy levels.⁵ Therefore, metallic clusters play a novel role in understanding the transition from molecules to nanoparticles.

In this context, computational studies can shed light on nanocluster chemistry. The use of a theoretical approach to finding the electronic structure of metal clusters was pioneered by Bonačić-Koutecký and co-workers.⁶ Similarly, Cheng and co-workers explored

$\text{Au}_{70}\text{S}_{20}(\text{PPh}_3)_{12}$ using the density functional theory (DFT).⁷ A clear picture of the Au-thiolate interface was revealed by Maksymovych *et al.*⁸ with the study on the adsorption of CH_3SH on the gold surface using scanning tunneling microscopy (STM) and DFT calculations. They discovered that the formation of linear RS-Au-SR binding motifs (‘R’ is an organic fragment) is favorable. The popular ‘divide and protect’ concept and the ‘superatom network model’ further helped to explore this field.⁹ Jadzinsky *et al.* and Daniel *et al.* reported the crystal structure of $\text{Au}_{102}(\text{SR})_{44}$ clusters and they observed that all 44 thiolate groups form RS-Au-SR motifs on the cluster surface.^{10,11} They named them ‘staple motifs’. This remarkable achievement provided atomic perception at the gold-thiolate interface. Therefore, it was accepted that ‘staple motifs’ were the preferred structures at gold-thiolate nanocluster surfaces. This finding is in contrast with the previously believed Au-thiolate protective polymer layer model.^{12,13} Over the years, in the quest for a more general structural rule, scientists discovered that the highly stable thiolate-protected gold clusters formed as a combination of a symmetric gold core and several protecting gold-thiolate ‘staple motifs’.¹⁴

In addition, the physical and chemical properties of small and large gold-thiolate clusters were investigated with DFT and compared with experimentally characterized systems.^{15–18} A major challenge is that the geometry of such ligated nanoclusters and associated energetics vary with the choice of theory and the robustness of the computational methods. So far, to the best of our knowledge, there is no report to help in choosing the proper theoretical methods for analyzing these systems. Thus, we searched for proper computational methods to examine gold-thiolate nanoclusters. We performed a benchmark analysis based on bond lengths (Au-S, Au-Au, and C-S, wherever applicable) and compared them against similar studies with the popular reference methods. Similarly, we benchmarked density functionals to predict the cluster stability in terms of relative energy. We used our analysis from benchmark study to predict the overall stability and ligand interaction energies of these nanoclusters. Thereby, we aspire to understand the behavior of popular density functionals on gold-thiolate

systems.

Alongside, we seek to establish a better description of the gold-sulfur bonding from a theoretical point of view. Earlier, a similar approach on gold-thiolate bonding was reported which interpreted the bonding interaction as covalent, ionic, or a combination of these two extremes.¹⁹ Nevertheless, a more in-depth quantitative analysis is required to understand the nature of bonds between gold and sulfur properly. In this pursuit, we performed theoretical analysis such as Quantum Theory for Atoms in Molecules (QTAIM),²⁰ Wiberg Bond Indices (WBI),²¹ Mayer bond order analysis,²² Natural Population Analysis (NPA),²³ and molecular orbital contribution analysis. Additionally, Energy Decomposition Analysis Based on Absolutely Localized Molecular Orbitals (ALMO-EDA) for bonded interactions²⁴⁻²⁶ helps us to describe the gold-sulfur interaction with sophisticated measures.

Computational Details

We have optimized all the starting geometries using 17 different density functionals and a wave-function-based method RI-SCS-MP2.²⁷ The density functionals cover the range from cheaper GGA methods to expensive double hybrid methods listed in Table 1.

Table 1: Density Functionals used for the benchmark study (**a**: DFT-D3 with zero-damping;²⁸ **b**: DFT-D3 with Becke–Johnson damping;^{28,29} **c**: DFT-D4³⁰).

GGA	meta-GGA	Hybrid-GGA	Hybrid meta-GGA	Range-separated Hybrids	Double-Hybrids
b BP86 ^{31,32}	a M06-L ^{33,34}	b B3LYP ^{35,36}	c PW6B95 ³⁷	ω B97 ³⁸	b B2PLYP ³⁹
c mPWPW ⁴⁰		c B3PW91 ^{35,36,41}	TPSSH ^b ^{42,43}	ω B97X-D3BJ ³⁸	
b B97-D ^{39,44}		c mPW1PW ⁴⁰	a M06 ^{33,34}		
b PBE ⁴⁵		b PBE0 ⁴⁶	a M06-2X ^{33,34}		
c revPBE ⁴⁷					

We have chosen four minima structures after optimization with RI-SCS-MP2/def2-TZVP (Figure 1). The frequency calculations on the optimized structures have confirmed them as minima with no imaginary modes. We have carried out single-point calculations with DLPNO-CCSD(T)^{48,49} on those optimized structures for benchmarking the DFT results on relative energy (RE) and thiolate interaction energy (TIE).

All the calculations are performed using ORCA 4.2.1 programme package⁵⁰ using a triple-zeta valence basis with one set of polarization function (def2-TZVP⁵¹). We have used effective core potential (def2-ECP)^{51,52} for chemically inert gold core electrons. Grimme’s empirical dispersion corrections (D3) with Becke–Johnson (BJ)damping^{28,29} and D4,³⁰ except for ω B97, were included. The functional ω B97X-D3BJ is the modified version of ω B97X-V with D3BJ correction by Najibi and Goerigk as implemented in ORCA. For M06-L, M06, and M06-2X, the older zero damping version of Grimme’s dispersion correction D3 is applied. We have used DFT-D4 dispersion correction for the functionals mentioned in Table 1 above because DFT-D3(BJ) is not available for those functionals in ORCA. We have used denser grid settings with angular grid Lebedev770 and the number of radial points 5.67 for DFT calculation and resolution-of-the-identity with the chain-of-spheres approximation (RIJCOSX)⁵³ to speed up the calculations.

Topological analysis is carried out on the first two minima shown in Figure 1 (**A** and **B**) using Multiwfn programme.⁵⁴ The wave function files for these calculations were generated by using the Gaussian 16 programme.⁵⁵ ALMO-EDA calculations for bonding interactions are conducted using Q-Chem software.⁵⁶ The canonical molecular orbitals are rendered using IQmol.⁵⁷

Description of the system

The extended X-ray absorption fine structure (EXAFS), X-ray diffraction (XRD), and wide-angle X-ray scattering (WAXS) studies^{58–61} have shown that in the majority of the gold-thiolate clusters, the ratio of the number of gold atoms and thiolate fragments are close to

1:1. Considering these experimental observations, we have proposed $\text{Au}_3(\text{SR})_3$ (where; $\text{R} = \text{CH}_3$) as the system for the benchmark analysis. This proposed structural formula comes with a simple cluster-like stoichiometry and closed-shell (spin multiplicity = 1) nature in the ground state. It enables us to avoid DFT spin contamination particularly in the open-shell systems, which will be dealt with in the future work.

Considering this, several trial geometries are generated from our chemical intuition with various orientations of Au and $-\text{SR}$. Preferred bonding interactions between gold and sulfur are the direct coordination between Au and S, bridging coordination where S is coordinated to Au–Au bond, and the capping coordination where S is coordinated simultaneously to 3 Au atoms in Au_3 ring, $(\text{Au}_3)\text{-S}$ as described by Kruger *et al.*¹⁵ We have started with eight different structures (Figure S1) made by intuitive modelling. All these geometries are optimized using density functionals and the reference RI-SCS-MP2 method. However, after optimization of the initial pool, we obtained four distinct minima (Figure 1) and considered them as the benchmarking data set. RI-SCS-MP2 optimized structures are taken as the reference geometries for further calculations on energy-related parameters. The lowest energy structures **A** and **B** are similar to an earlier theoretical study on gold-thiolates.^{62,63}

Description of the database

We carried out benchmark studies to calibrate the accuracy of geometry optimization, relative energies (RE) of the stable structures. From a dataset of four minima (Figure 1), we have discussed the benchmark analysis in terms of their normalized mean absolute error (NMAE). NMAE values obtained from the density functional methods are taken for comparison against the reference wave function-based methods. We have considered the density functional with NMAE less than 0.40 as a good performer for geometry optimization and NMAE less than 0.20 for relative energies. In our calculation, RI-SCS-MP2/def2-TZVP is the reference method for the benchmark study on geometry optimization, whereas single

point energy from the DLPNO-CCSD(T) calculation is the reference for the RE.

$$MAE_j = \frac{1}{N} \left[\sum_{i=1}^N |x_i - x_{ref}| \right] \quad (1)$$

$$NMAE_j = \frac{1}{\max(MAE_j)} [MAE_j] \quad (2)$$

Where, x_i is i^{th} value of a parameter such as BL and RE; the x_{ref} is the i^{th} value of the parameter with reference method; N is the total number sampling for a particular parameter in a specific method, j.

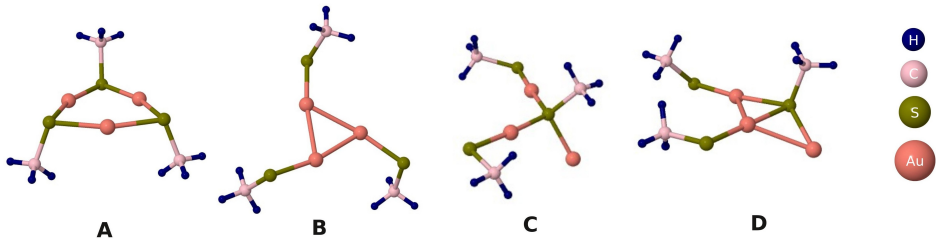


Figure 1: Stable structures optimized with reference RI-SCS-MP2/def2-TZVP level of theory.

Geometry Optimization

We have obtained structures **A**, **B**, **C**, and **D** after optimizing the trial geometries (Figure S1) with the RI-SCS-MP2 method. Similarly, we have optimized all these trial geometries in all the functionals we have considered in this study. While all the density functionals have yielded **A**, the structures **B** and **C** are obtained only with some of the density functionals. Using the DFT methods where structure **B** and **C** are not found after the first optimization run, we have used the optimised geometries of **B** and **C** from the RI-SCS-MP2 optimization as a guess for re-optimizations in these DFT methods. In addition, we do not obtain **D** with any of the DFT methods starting from the initial pool (Figure S1). Therefore, we reoptimized the **D** with each of the DFT methods to see whether that minima is stable under the DFT optimization.

We have considered the bond lengths in **A** and **C** as the geometry parameters for the benchmark. Optimized parameters of **B** are not taken as they are not recovered with some of the DFT methods (see result and discussion section). RI-SCS-MP2 is considered as the reference for bond lengths because those are fairly comparable with literature values mentioned in some of the pioneering works.^{15,64,65} We have examined and categorized similar geometries and reported the bond lengths (Table S1, S2, and S3). A plot of the three different bond lengths of structure **A** is shown in Figure S2. The NMAE values for each method are calculated and plotted in Figure 2a.

Calibrating the accuracy as mentioned above gives us the information for selecting the best DFT method. However, we also need to consider the computational cost – the other dimension of performance. Hybrid density functionals are often used to obtain reliable geometries, but they also have much larger computational costs (Table S4). Therefore, we include the cost factor in choosing the best functionals for gold-thiolate systems that are much larger than our candidate molecules ($\text{Au}_3(\text{SMe})_3$).

We analyzed the variation of the NMAE values against the computational time. To obtain that, we have presented the plot for the expense of computation in terms of NMAE values of BL vs. optimization run-time in Figure 3. The reported computational time is from the calculations performed in a dual socket Intel Xeon SKL G-6148 (2.4 GHz) compute node using 40 processors. MaxCore (memory) value is set to 3000 MB in orca input file for each calculation. A sample input file is provided in supplementary information.

Relative Energy (RE)

For a particular molecular structure, e.g., **A**, the minimum at each computational level of theory is slightly different from each other. To calibrate the energy, it is a common practice to compute energy (single-point calculations) at various levels on the same geometry. This reference geometry was chosen to be the structures optimized at RI-SCS-MP2/def2-TZVP. We have computed the energies of four minima structures (Figure 1) with all the DFT

methods under consideration. The relative energy (RE; in kcal mol⁻¹) of the structures (**B**, **C**, and **D**) is estimated as their energy difference with **A**. For example, $RE(\mathbf{B}) = E(\mathbf{B}) - E(\mathbf{A})$, where $E(\mathbf{A})$, and $E(\mathbf{B})$ are the total energies of **A** and **B**.

The RE (in kcal mol⁻¹) of **B**, **C**, and **D** at various DFT methods are shown in Figure S3 and Table S5. Figure 2b shows a relative NMAE plot considering DLPNO-CCSD(T) energy as the reference.

Results and discussion

We first discuss the benchmarking of the density functionals for gold-thiolate nanoclusters on geometry optimization, relative stability, and thiolate (ligand) interaction energies (TIE), followed by the bonding analysis for a better understanding of the nature of gold-sulfur interaction.

Benchmarking

Geometry Optimization

Geometry optimization with *ab-initio* methods is often prohibitively expensive due to various reasons. Energy evaluations are considerably more expensive than DFT methods. Many of the efficient approximate methods lack analytical gradients, and hence the gradient evaluations are even more expensive. As the iterative geometry optimization would take several optimization cycles of energy and gradient evaluations, finding a suitable method for geometry optimization is the most crucial task for our study. Therefore, our goal here is to compare the reliability, reproducibility, and efficiency of the results on bond lengths – Au-S, Au-Au, and C-S – for structures **A**, **B**, and **C**.

Compared to the reference RI-SCS-MP2 method, the NMAE plot (Figure 2a) shows that two hybrid-GGA functionals mPW1PW and PBE0 performed similarly well with the least NMAE (~0.27) in the series. Computationally costly double hybrid functional B2PLYL

also gives the same NMAE (~ 0.27) as these two functionals followed by hybrid-meta-GGA functional TPSSh (~ 0.29) and another hybrid-GGA B3PW91 (NMAE ~ 0.31). Although TPSSh trails behind in NMAE, we have noticed that it produces d_{Au-Au} very close to the d_{Au-Au} from the RI-SCS-MP2 method, while d_{Au-S} is overestimated by most of the density functionals (Table S1, S2, and S3).

In the GGA range, PBE shows the best performance (NMAE of 0.36) followed by mPWPW (0.38). Comparatively, the most popular hybrid-GGA functional B3LYP in this study show less accuracy (NMAE ~ 0.62) than three of the GGA functionals. Although BP86 is the computationally cheapest functional in this series (Figure 3), this functional do not show good performance (NMAE ~ 0.42) – two of the GGA functionals have better accuracy than BP86. The two range separated hybrid functionals ω B97 and ω B97-X(D3BJ) show nearly similar results as the GGA functionals but they take longer time to optimize the structures as reflected in Figure 3. Minnesota functionals are not in our recommendation as their accuracy on bond lengths are far less than the above recommended functionals with MO6-2X showing the highest NMAE value amongst all. Thus, this analysis shows that the GGA methods are good for geometry optimization.

The GGA functionals (mPWPW, PBE, BP86, revPBE, and B97D) and double-hybrid functional B2PLYP have provided **B** and **C** after optimizing the initial pool, whereas the other functionals are prone to converge to **A**. Hence, we can conclude that **A** is the most abundant and also the most stable structure among the four (Figure 1). This idea is further reinforced from RE and TIE analysis. It also confirms the reliability of GGA functionals for the geometry of gold-thiolate clusters as found by Gronbeck *et al.*¹⁷ Table S3 shows that **C** is stable under all DFT optimizations, whereas **B** is not recovered with M06, M06-2X, M06-L, ω B97, and ω B97X-D3BJ density functionals (Table S2).

After calibrating the DFT functionals for accuracy, we have analyzed the computational cost for optimizations. Although mPW1PW and PBE0 give the most reliable structures, as Hybrid-GGA functionals, it is more costly to optimize the geometries with these two. Hence,

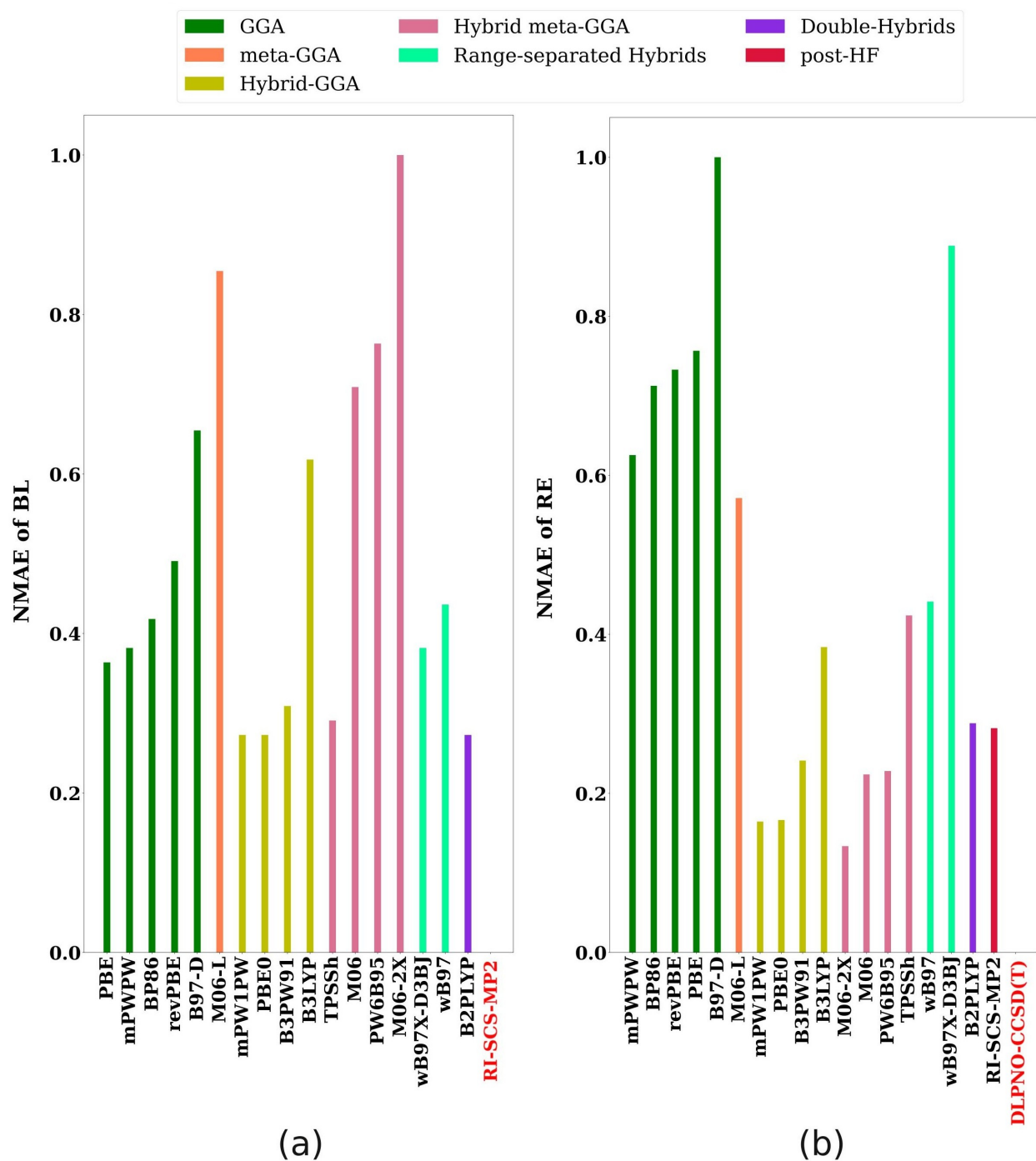


Figure 2: NMAE obtained at various level of theory for (a): bond length and (b): relative energy.

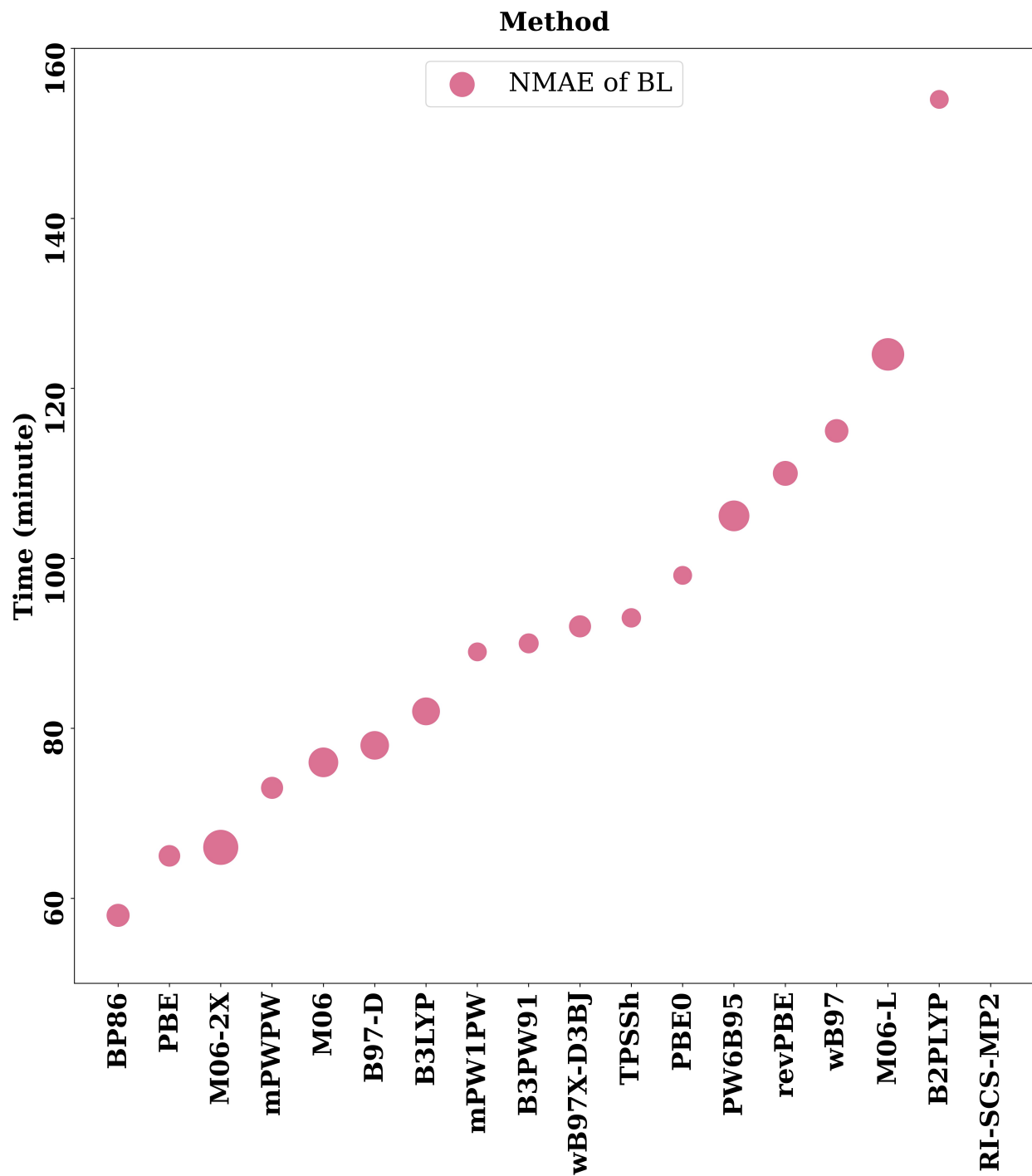


Figure 3: The optimization run-time against the computational methods with NMAE of BL values represented as the area of the circles.

if large number of optimizations are involved, these two are less preferred over the accurate GGA functionals (see above). PBE spends the least time optimizing the structures, thereby turning out to be an excellent functional in terms of computational cost and accuracy as described in Figure 3 and Table S4. Our observation reinforces the study by Kruger *et al.*¹⁵ where the acceptability of GGA methods are predicted for gold-sulfur interactions, however, the ‘revised’ version of PBE functional, revPBE and another GGA functional B97-D show significantly weak results in this case. In GGA range, revPBE has converged to the **A** after 125 optimization cycles (highest amongst GGAs), whereas B97-D spends the highest length of time to locate the minima (Table S4).

Overall, the best cost-accuracy is shown by PBE and mPWPW for optimization – the PBE is more accurate and it’s faster than mPWPW with exactly same number of optimization cycle (80) to find the minima. BP86 is the fastest in this series with same number of optimization cycle as PBE and mPWPW, but it lacks accuracy.

Relative Energy (RE)

This section illustrates the strength of the density functionals to find the relative stabilities of the optimized structures through a benchmark analysis. The previous discussion shows the robustness of the GGA density functionals on the reproducibility of the geometries. Although, we cannot firmly conclude that the GGA functionals’ performance also holds for understanding the relative stability of the structures. A proper way to test this is to look for the NMAE of RE calculation with each of the density functionals.

Considering DLPNO-CCSD(T) energies as the reference (Figure 2b), all the GGA functionals have significantly high NMAE values. Therefore, no GGA method is recommended for predicting the relative stability of gold-thiolate nanoclusters. In contrast to the performance for geometry optimization, M06-2X has the best results with the lowest NMAE ~ 0.13 among all the functionals in terms of RE. M06 also shows improvements (NMAE ~ 0.22) over its performance in geometry optimization, however, M06-L lacks significantly in both cases.

Hybrid-GGA functional PBE0 and mPW1PW keep excellent performance in terms of RE with same NMAE value ~ 0.17 . Hence, we have concluded that PBE0 and mPW1PW have the most consistent result considering both geometry optimization and RE.

Nevertheless, a clear distinction in the performance of PW6B95 can be made from Figure 2a and 2b. Performance of this meta-hybrid density functional is not recommended for predicting the geometries of the structures. But here, PW6B95 has improved NMAE (~ 0.23) followed by the hybrid-GGA B3PW91 (~ 0.24). The performance of B2PLYP and ω B97 have not altered much from their respective accuracy in geometry. B2PLYP shows comparable performance with respect to RI-SCS-MP2, however, that is far from our acceptance cut-off for RE. Similarly, range separated hybrid ω B97-X(D3BJ), hybrid-meta-GGA functional TPSSh, and popular hybrid functional B3LYP are not reliable performers in this context. Considering all, we strongly recommend M06-2X for relative stability and energetics study of the gold-thiolate nanoclusters.

Stability Analysis

In addition to the error analysis with NMAE, the trend in relative energies in various functionals among the four geometries is important. The order of stability is **A** > **B** > **C** > **D** in RI-SCS-MP2, while in DLPNO-CCSD(T) the order is **A** > **C** > **B** > **D** (Figure S3 and Table S5). Density functionals such as PBE, B2PLYP, BP86, revPBE, mPWPW, PW6B95, and B97D follow the RI-SCS-MP2 trend. This order of RE indicates a strong Au-Au interaction over the capping Au₃-SR interaction. Hence, GGA methods favor the Au-Au orbital overlap and suggest the stability of a singly coordinated system over the three-folded coordination.

Similarly, a trend in relative energy from the DLPNO-CCSD(T) calculation is consistent with hybrid-DFT functionals such as B3LYP, PBE0, mPW1PW, M06-2X, and B3PW91. According to this, it predicts the higher stability of structure **C** with a strong capping sulfur interaction over weaker Au-Au interaction as shown in Figure 1. Thus, the hybrid methods and range separated method ω B97 are more likely to disfavor the extent of Au-Au orbital

overlaps of the Au trimer and suggest that the tri-coordinated system to be more stable than the singly bonded thiolate coordination in gold-thiolate nanocluster.

We have observed two different trends in relative energies – one with RI-SCS-MP2 and another following DLPNO-CCSD(T). In between these two reference methods, we have considered DLPNO-CCSD(T) as the reliable reference for the stability and interaction study. This is because it not only recovers 99.9% of the CCSD(T) correlation energy within DFT comparable timescale,^{48,49} but also reinforces the Au-S interaction over Au-Au interaction which is also supported from experimental studies.^{15,64,65}

However, relative energy only stands for molecular stability as an overall description considering all kinds of interactions, whereas ligand interaction energy provides sophisticated information on the metal-ligand coordination and corresponding stability. The Thiolate Interaction Energy(TIE) is a useful property to predict reactions mechanisms involving gold-thiolate clusters, energetics of cluster formation, and degradation. Therefore, TIE has a much precise insight to validate our results obtained from the benchmark studies on the robustness of the density functionals.

The TIE is considered as the interaction between the gold atoms and the thiolate fragments. We have made Au₃ fragments and (SR)₃ ligand fragments from each of the four minima (Figure 1). We have calculated the single point energy on each fragments separately with the recommended density functionals from the RE benchmark study – M06-2X, M06, PBE0, and mPW1PW. We have evaluated TIE (in kcal mol⁻¹) using equation 3 taking the reference method as DLPNO-CCSD(T).

$$\Delta E_{TIE} = [E_{Au_3(SR)_3} - (E_{Au_3-fragment} + E_{(SR)_3-fragment})] \quad (3)$$

The ΔE_{TIE} is computed for each geometry at these five methods (see above) and is plotted in Figure 4.

In general, a significant negative interaction energy stands for high stability from gold-thiolate interaction, confirmed by lower TIE of 30.45 kcal mol⁻¹ for **A** than the TIE for **C** as

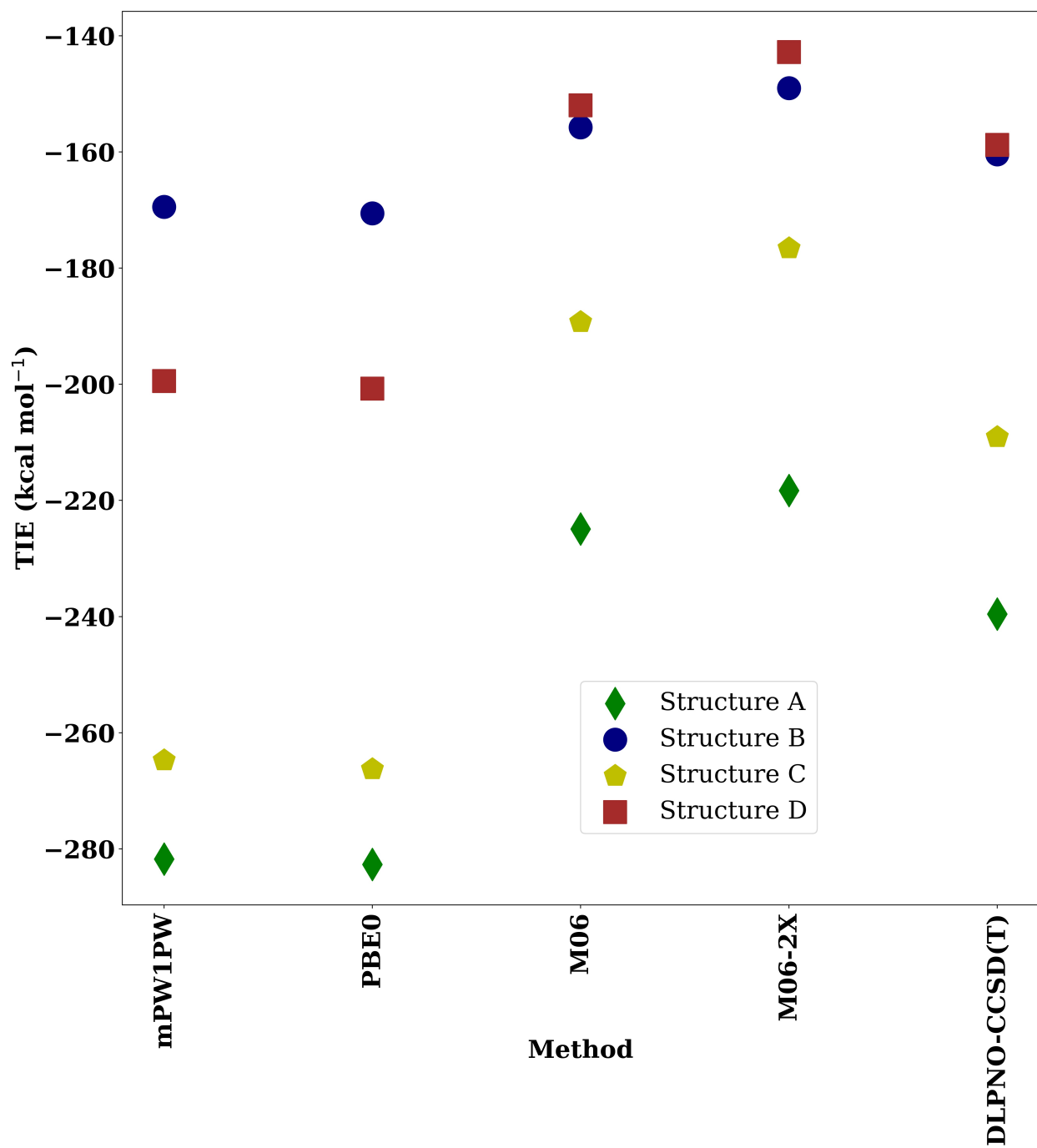


Figure 4: Thiolate interaction energy for the four structures in kcal mol⁻¹.

per the DLPNO-CCSD(T) energies (Figure 4 and Table S6). Besides, **C** has 48.68 kcal mol⁻¹ lower TIE than **B**, and the latter has only 1.65 kcal mol⁻¹ lower TIE than **D**. Table S5 also represents a slight RE difference for the structures **B** and **D**. This comparison also provides an excellent argument on the directional nature and covalency of the Au-S bond as described by Kruger *et al.*¹⁵ M06-2X and M06 depicts the relative TIE pretty comparable to the DLPNO-CCSD(T) calculation, followed by hybrid-GGA functionals PBE0 and mPW1PW. However, the later two represent a smaller gap in TIE between **A** and **C** and significantly larger difference in TIE between **B** and **D** than M06-2X, M06, and DLPNO-CCSD(T) results. A Lower TIE also stands for better Au-S orbital interactions by imposing proper metal-ligand orbital overlap. Our study shows that the bridging sulfur (Au-S-Au) interaction is more favorable over the single bond (Au-S) and capping sulfur (Au₃-S) interactions as shown in Figure 1. This inference is in line with an earlier study by Letardi *et al.*¹⁶ The experimental and theoretical studies also stand for the bridging Au-S-Au bonding.^{8,66-68}

Bonding

Research on Au-S bonding has gained a plethora of interest among the scientific community. Despite numerous experimental investigations, the bonding picture seems to have quite a diversified profile of its own.

Topological analysis

To interpret the gold-gold interaction (Au-Au) and gold-sulfur interaction (Au-S), we have performed QTAIM²⁰ analysis on **A**, **B**, and the isolated fragment of AuSR (R=CH₃) for comparison. A color-filled map of Electron Localization Function (ELF) is shown for AuSCH₃ in Figure 5a, **A** in Figure 5b, and **B** in Figure 5c. The electron sharing among the atoms Au and S is lower in **A** and **B** compared to the sharing between Au and S in AuSCH₃.

The analysis of bond paths and critical points in the Laplacian of electron density ($\nabla^2\rho(\mathbf{r})$) within the QTAIM framework helps us to identify the bonding between the atoms. The

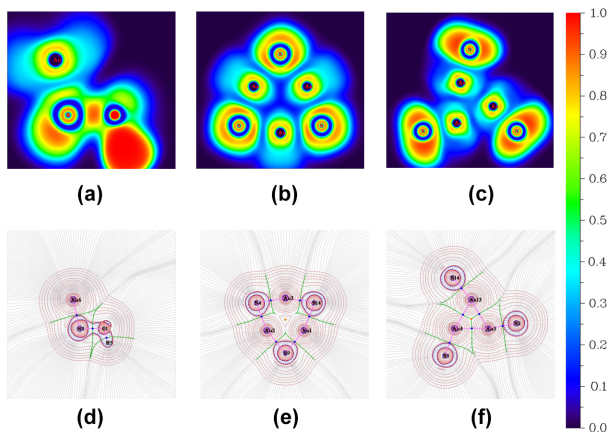


Figure 5: The top row shows color filled map of electron localization function (ELF) for AuSCH₃ (5a), **A** (5b), and **B** (5c). The bottom row depicts the Laplacian of electron density plot for AuSCH₃ (5d), **A** (5e), and **B** (5f). Calculations obtained at M06-2X/def2-TZVP level of theory. For clarity, only Au and S atoms are shown here.

$\nabla^2\rho(\mathbf{r})$ is plotted for isolated AuSCH₃ molecule in Figure 5d, for **A** in Figure 5e, and for **B** in Figure 5f. The red and blue lines show the charge depletion and charge accumulation, respectively. The pink lines show the bond paths connecting the atoms. The blue dots are bond critical points (BCP), and the orange dots are ring critical points (RCP). The RCP links three S atoms for **A** and three Au atoms in **B**. The bond paths do not show the bonding between Au atoms in **A**.

We examined the details of the topological parameters, Table S7 for AuSCH₃, Table S8 for **A**, Table S9 for **B**, to understand the nature of the Au-Au and Au-S bonding. The topological parameters Lagrangian kinetic energy $G(\mathbf{r}_c)$, potential energy density $V(\mathbf{r}_c)$, energy density $E(\mathbf{r}_c)$, $H(\mathbf{r}_c)$, $-G(\mathbf{r}_c)/V(\mathbf{r}_c)$, $G(\mathbf{r}_c)/\rho(\mathbf{r}_c)$, and the Laplacian of electron density ($\nabla^2\rho(\mathbf{r}_c)$) at the critical points are given there.

The $\rho(\mathbf{r}_c)$ at BCP for C-S bond is 0.1730, the highest among all other $\rho(\mathbf{r}_c)$'s. A higher value of $\rho(\mathbf{r}_c)$ and a negative $\nabla^2\rho(\mathbf{r}_c)$ at the BCP suggest that⁶⁹ S-C bond is covalent in all the three cases. However, Au-S has a positive $\nabla^2\rho(\mathbf{r}_c)$ and a smaller value for $\rho(\mathbf{r}_c)$. Together, they fail to provide a straight-forward description of the nature of the Au-S and Au-Au interactions (Table S8 and S9). A positive $\nabla^2\rho(\mathbf{r}_c)$ suggests electron depletion at

BCP which we can see from the respective diagrams (Figure 5d, 5e, and 5f).

Analysis based only on $\rho(r_c)$ and $\nabla^2\rho(r_c)$ suggest a ‘closed-shell’ type of bonding⁶⁹ with a smaller $\rho(r_c)$ (0.0711) between Au atoms, while a moderate $\rho(r_c)$ (0.1050 in **A** and 0.1280 in **B**) implies a charge-shift interaction between Au and S atoms. The $\rho(r_c)$ in **A** is lower where the S is bonded with two Au atoms. However, these results including Au atoms can be deceptive because the classification based on $\nabla^2\rho(r_c)$ is shown to be consistent with main group elements, while this assignment is not robust for atoms with atomic shell structure beyond Ar ($Z=18$). Moreover, this interpretation does not entirely discriminate between covalent and ‘closed-shell’ interactions.

Therefore, we have considered other descriptors to understand the Au-S and Au-Au interactions. All the $H(r_c)$ values are less than zero⁷⁰⁻⁷² and $-G(r_c)/V(r_c)$ within the range 0.5 to 1.0⁷³ for all three cases, suggesting some covalent character in these bonds. Another indicator, a value greater than two for $|V(r_c)|/G(r_c)$, implies that the potential energy is dominant, the interaction is of shared-shell type, and the bond is covalent. For C-S bonds, $|V(r_c)|/G(r_c)$ is 3.26 and 3.29 in **A** and **B** confirming all the previous assertions as a covalent bond.

For Au-S and Au-Au bonds, the values of $|V(r_c)|/G(r_c)$ are between one and two ($\approx 1.33-1.53$) – i.e., $G(r_c) < |V(r_c)| < 2G(r_c)$ – suggests that the potential energy is the dominant factor. The bond degree $H(r_c)/\rho(r_c)$ is negative for both Au-Au and Au-S bonds, although lower than the value for C-S bond (-0.6532), indicating shared-type interaction.

The Au-Au bond paints a different bonding nature, as seen from Table S9. Both $\rho(r_c)$ and $V(r_c)$ drop significantly as compared to the Au-S bond signifying a large depletion of electron density in between Au and Au atoms. However, the potential energy (-0.0760) slightly surpasses the kinetic energy (0.0571), thereby representing a weak ‘closed-shell’ type interaction. Another covalency descriptor, $G(r_c)/\rho(r_c)$, has values slightly less than one, indicating that Au-S and Au-Au bonds are partially covalent (Table S8 and S9).

The bond degree (BD) of singly coordinated Au-S of **B** is ≈ -0.48 and for the doubly

coordinated Au-S of **A** BD is less negative, ≈ -0.39 . It corresponds to the decrease in Au-S bond covalency in **A**. Comparatively higher $\rho(r_c)$ (0.1280) and lower $\nabla^2\rho(r_c)$ (0.1170) for **B** emphasizes the aforementioned observation. Depletion of electron density at BCP of Au-S bond in **A** is supported by a significant decrease in $\rho(r_c)$ (0.1050) and increases in $\nabla^2\rho(r_c)$ (0.1470) than **B**. Hence, the two-fold coordinated Au-S bond (Au-S-Au) (in **A**) has a much weaker covalent character than the singly coordinated Au-S bond (in **B**). The values of another descriptor, $|V(r_c)|/G(r_c)$, for bridging and singly coordinated Au-S bond are ≈ 1.53 and ≈ 1.68 , respectively. Therefore, potential energy is the dominant factor in case of singly coordinated Au-S bond, inferring a higher covalent character as compared to the bridging Au-S.

From these analyses, we conclude that the interactions between Au-S and Au-Au are not standard covalent types. An in-depth analysis of electronic population and energy decomposition is required for further understanding.

Natural Population and Bond Indices

To further examine the nature of Au-S and Au-Au bonding, we have conducted the Natural Population Analysis (NPA).²³ The natural charges on Au, S, and C atoms from NPA analysis are given for the isolated AuSCH₃ molecule (Table S13), **B** (Table S14), and **A** (Table S15). First, we have analyzed the charge distribution in the basic fragment, the AuSCH₃ molecule. The Au atom has a small partial positive charge, ($+0.15e$ in AuSCH₃, and the S atom has an even smaller partial negative charge ($-0.07e$) and CH₃ carry the remaining $-0.08e$. C has the highest partial charge of $-0.7e$.

A reduction in electronic charge from H $1s$ orbitals is seen which results in an overall increase in the $2p$ electronic population of the C atom as represented in Table S16. Besides, S $3p$ population increased significantly due to charge transfer from filled Au $5d$ orbitals. Au $6s$ orbital remains almost inert in this case, suggesting a practically non-existing $s-d$ hybridization. However, a small increase in Au $6p$ population may infer an Au $d-p$ orbital

mixing. The back-donation from the filled-orbitals of S to vacant Au $6p$ orbital is ruled out due to poor overlap integral of the participating orbitals. The ELF and Laplacian of electron density (Figure 5a and 5d) for the AuSCH₃ also show a small amount of electron sharing in between Au and S. Thereby, we can ascertain that in AuSCH₃ molecule, Au $5d$ electrons are being shared to S $3p$ orbital. Table S10 show higher than the single covalent bond in between Au and S atoms (WBI value is 1.4 for Au-S bond).

B is visualized as comprising of three AuSCH₃ fragments. Another way to visualize is to consider three -SCH₃ ligands coordinated to the central Au₃ ring – a gold cluster passivated by the ligands. The charge distribution is similar to AuSCH₃ (Table S14). A slight drop in positive charge on Au atoms (+0.13 e) followed by a slight reduction of negative charge over the S atoms (-0.06 e) with respect to the AuSCH₃ molecule (Table S13). The charge on CH₃ is increased to -0.21 e . The slight reduction in positive charge on Au atoms is attributed to cluster formation, where the electron density is shared among the Au atoms of the trimer (see the ELF plot in Figure 5c). The BCP analysis ensures the existence of Au-Au weak partial covalent bonding between the gold atoms in the Au trimer core.

The Natural Electronic Configuration (NEC) analysis (Table S17) shows a considerable rise in Au $6p$ population (0.25) and a substantial drop in Au $5d$ population (9.65). Au $6s$ electrons start to engage in bonding interactions at this point resulting in an $s-d$ hybridization. Thus, a possible $5d-6p$ mixing is observed within the Au atoms. An Au $s-d$ hybridization stabilizes the Au-S bond. Therefore, the change in Au hybridization (by increasing the s character) leads to higher electronegativity and thereby less electron sharing with the adjacent S atoms. This condition is further reflected in the lowering of overall electronic charge on S atom than that of molecular AuSCH₃. The bonding between C and S is covalent, justified by WBI analysis (Table S11). The Mayer bond order analysis is also consistent with the NPA and NEC analyses. Together, they suggest a partial covalent interaction between Au and S and Au and Au atoms.

In the case of **A**, an NPA analysis reflects an overall increase in the positive charge on

Au atoms (+0.16 e), followed by an increase in the negative charge on S atoms (-0.11 e) with respect to **B**. The natural charges on CH₃ group is -0.15 e . An increase in Au positive charge (Table S18) infers a decrease in overall Au $6p$ population followed by a substantial increase in the electron density in $5d$. Also, a significant drop in Au $6s$ electron density is noticeable here. This situation is best described in terms of an increase in Au $s-d$ hybridization.

In short, the BCP analysis has revealed no existing bond paths between Au and Au atoms in **A**, which is reflected in the lower Au-Au electron sharing. Au $6s$ orbital plays a significant role by introducing a higher s contribution in Au hybrid orbitals to make the bridging S coordination feasible. However, a substantial flow of electronic charge from Au to S $3p$ (to some extent to the vacant S $3d$) is also prevailing here. Likewise, a lower electronegativity difference between S and C atoms leads to electronic charges residing mostly on the C atom. The respective WBI and Mayer bond order (Table S12) confirmed the two-fold bridging-S configuration of **A**.

Canonical Molecular Orbitals

Occupied canonical molecular orbitals of **A** and **B** are shown in Figure 6 and 7. The HOMO orbitals entirely comprise Au-S antibonding interactions along the Au-S bond axis (Figure 6). MO-11 to MO-23 show bonding interaction between Au and S orbitals and Au and Au orbitals. On the other hand, the antibonding interaction between the same is also occupied (HOMO to MO-3). Therefore, the covalent interaction between Au and S orbitals is small, substantiating our understanding from earlier AIM analysis that a weak covalent interaction exists between Au and S atoms. Au-Au interaction is also largely disfavored as the antibonding orbitals are occupied, drawing the bond order close to zero.

Figure 7 shows bonding overlap between Au and S and Au and Au orbitals in MO-12 to MO-23. These interactions include σ and π type bonding, whereas HOMO to MO-11 shows Au-S and Au-Au antibonding interactions. As both the bonding and antibonding orbitals of Au-S fragments are occupied, it suggests that the extent of covalent bonding between the

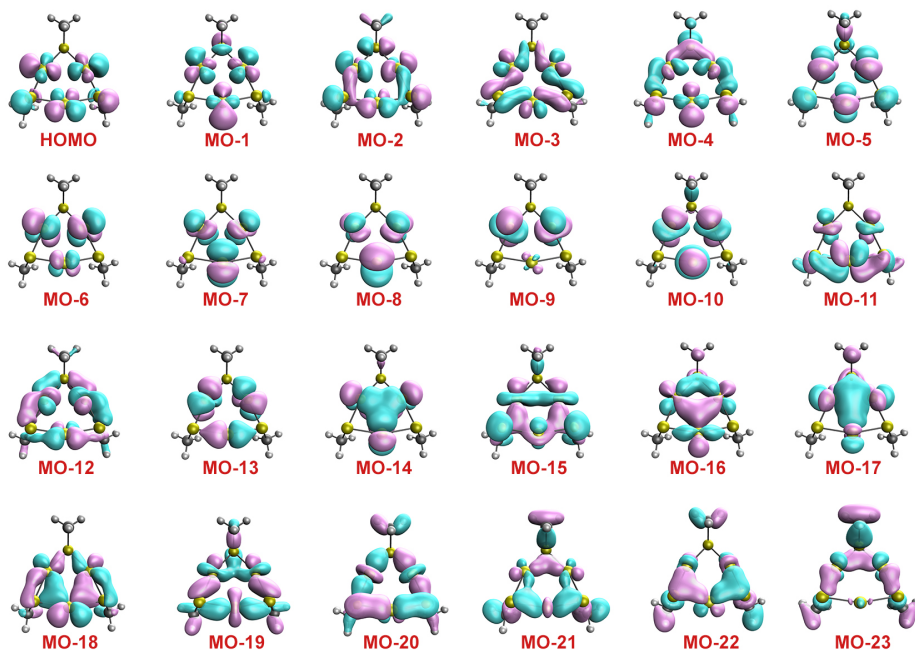


Figure 6: Canonical Molecular Orbital diagram for **A** obtained at M06-2X/def2-TZVP level of theory.

Au and S and Au and Au atoms is small. However, the overlap is much pronounced for Au-S interaction in case of **B**, signifying the singly coordinated Au-S bond experiences greater covalent type interactions than that of the bridging Au-S bond in **A**.

In Table S19 and S20, the LUMOs show a higher fragment contribution from the S-C bond. Hence, the Au-S bond stability does not arise from the overlap of atomic orbitals. It stems from the charge transfer assisted interactions earlier supported by NPA. Molecular orbital analysis for **A** and **B** shows that the occupied-orbitals are primarily composed of Au *s-d* hybrid orbitals and S *3p* orbitals. Moreover, **B**, which has a singly-coordinated ligand system to each Au atom, shows *s-d* mixing (Table S19), further strengthening our understanding from the previous NPA study (Table S16). Au *d* orbitals are dominant here, which interacts with S *p* orbitals to facilitate the charge transfer. On the other hand, **A** shows the significant contribution from Au *6s* orbital in HOMOs, thereby imposing a higher Au *s-d* mixing (Table S20). Higher Au *s-d* mixing stabilizes the Au-S bond by increasing charge transfer as reflected in NPA (Table S15). This kind of interaction surpasses the Au-Au

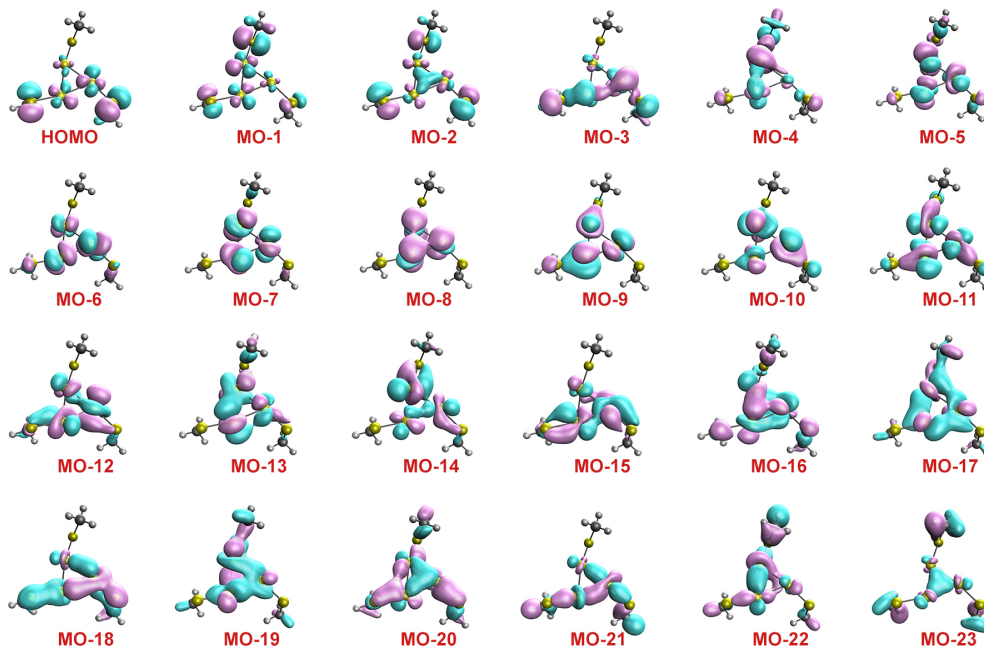


Figure 7: Canonical Molecular Orbital diagram for **B** obtained at M06-2X/def2-TZVP level of theory.

aurophilic interaction and results in Au-S-Au two-folded coordination.

ALMO-EDA

We have carried out an energy decomposition analysis (EDA) for the Au-S bond of **B**. EDA approach helps to understand the chemical bonds ranging across nonpolar, polar, ionic, and charge-shift bonds. We have estimated the stabilization from spin-coupling, polarization and charge transfer, and destabilization from Pauli repulsions. In variational EDA, the bonding interaction term is the difference between the DFT calculation on the entire molecule and the sum of DFT calculations on the separately optimized, isolated fragments. It is described with the equation 4.

$$\begin{aligned}
 \Delta E_{int} &= E_{molecule} - \sum_Z^{frags} E_Z \\
 &= \Delta E_{PREP} + \Delta E_{FRZ} + \Delta E_{SC} + \Delta E_{POL} + \Delta E_{CT}
 \end{aligned}
 \tag{4}$$

ΔE_{PREP} is the energy required to distort each radical fragment to the desired geometry in its bonded state ΔE_{GEOM} and orbital rehybridization energy ΔE_{HYBRID} . ΔE_{FRZ} is the energy change leading to the two radical fragments interacting without undergoing spin-coupling (SC), polarization (POL), or charge-transfer (CT). This term is entirely a nonbonded interaction for a triplet state and is typically repulsive due to Pauli’s repulsion. It comprises interactions from inter fragment electrostatics, Pauli repulsion, exchange-correlation, and dispersion.⁷⁴ ΔE_{SC} is the energy difference coming from switching the spin of the two radical electrons from high-spin triplet to low-spin singlet. This term is typically attractive associated with covalent bond formation. ΔE_{POL} comes from the low-spin orbital relaxation because of the presence of the field of the other fragment. ΔE_{POL} term includes contributions from electric polarisation and orbital contraction. However, the orbital contraction term is insignificant in the case of heavier elements.²⁴ The final ΔE_{CT} term corresponds to the movement of electrons within the fragments.⁷⁵

Covalent, and charge-shift bonds have relatively high ΔE_{SC} , polar bonds have relatively high ΔE_{POL} , and charge-shift and ionic bonds have relatively high ΔE_{CT} . Thus, ALMO-EDA interfaces classical bonding concepts with quantum mechanical methods.⁷⁶ So, the general question is how we can use this approach to understand the Au-S interaction. To do that, we have invoked the KS-DFT approach in our EDA calculation. Figure 8 represents such analysis considering M06-2X functional with def2-TZVP basis set. As in the ALMO-EDA approach, bonded interactions are only limited to single bonds. Therefore, we cannot account for the bonding nature of **A** where S shares a two-folded coordination. Hence, in our case, we have considered only an isolated AuSCH₃ molecule and **B**.

Figure 8 shows that the ΔE_{SC} term is the most stabilizing factor for an isolated AuSCH₃ molecule. Relatively higher SC energy infers covalent and charge-shift bond.²⁴ Dispersion plays only a modest role in both cases as no bulky R-group is present. A significant contribution of charge-transfer is evident from Figure 8 and NPA analysis in Table S13. However, stability due to polarisation is marginal here. This result is also accountable from NEC anal-

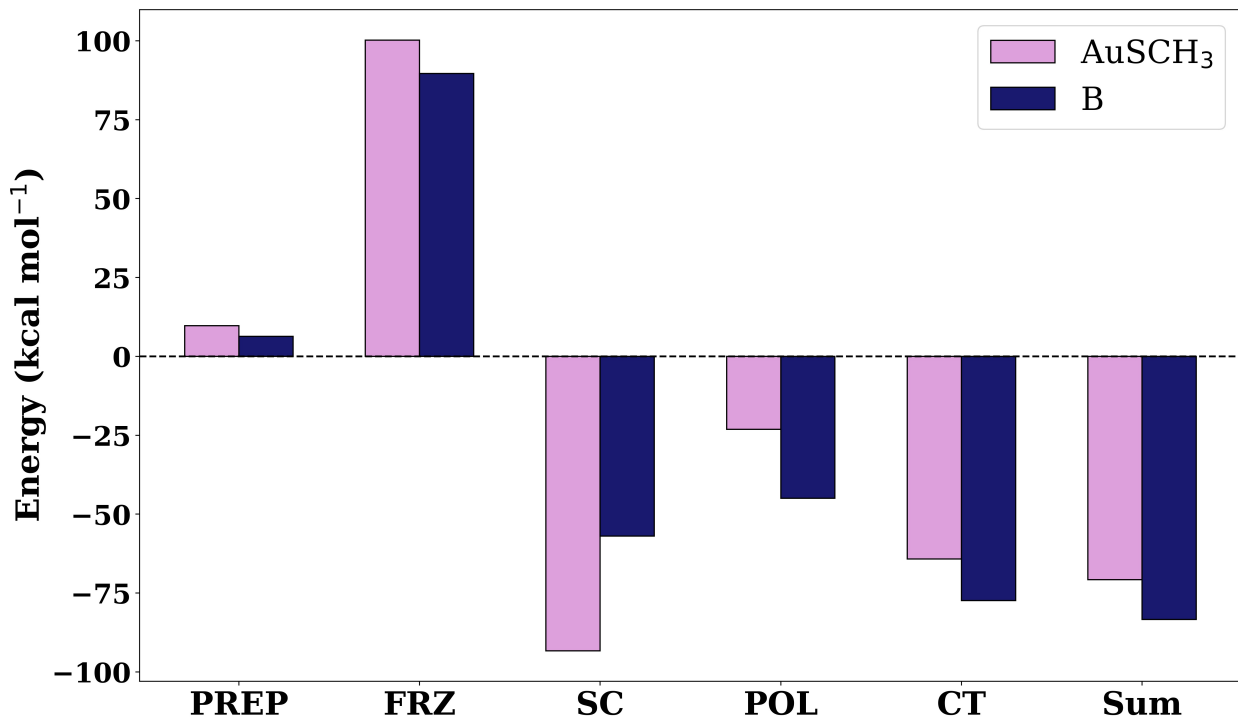


Figure 8: A comparison of the EDA terms obtained with different density functionals for the Au-S bond of isolated AuSCH₃ and **B**.

ysis in Table S16, which shows no Au *s-d* hybridization. Participation of Au *5d* electrons results in a hybrid covalent-CT stabilization analogous to a charge-shift bond.⁷⁵

Additionally, Figure 8 infers that the charge-transfer term ΔE_{CT} is dominant in the Au-S bond of **B**, followed by a higher stabilization from polarisation, ΔE_{POL} . QTAIM analysis has already revealed that the bond enjoys a partial covalent character, while charge transfer from Au to SCH₃ ligand is depicted in previous NPA studies. A moderate $\rho(r_c)$ and a positive $\nabla^2\rho(r_c)$ value suggest a ‘closed-shell’ interaction much like ionic or charge-shift bonds. The stabilization from ΔE_{POL} term is attributed to the electronegativity-induced polarisation effect causing electron flow from Au to SCH₃ ligand.

In brief, the Au-S bond in **B** is stabilized from an electronegativity-controlled polarisation, strengthening the partial covalency between Au and S atoms. Increasing Au *s-d* hybridization in the cluster leads to a higher polarisation in Au-S bond than isolated AuSCH₃ molecule. High Pauli repulsion due to a poor orbital overlap between Au and S atoms reduces

the overall covalent interaction. Charge transfer from gold cluster to thiolate ligands thus occurs as a stabilizing factor against this effect. The Charge-shift and ionic bonds generally show high CT energies. The increase in POL and CT stabilization energies induce more electronic charge to flow from Au to SCH₃ ligand, which is reflected in the NPA (Table S14) and NEC analysis (Table S17).²⁴ Therefore, we can conclude that the Au-S bond in gold-thiolate nanoclusters acts as a charge-shift bond, in which the ionic structure contributes profoundly.

Conclusions

In general, the benchmark study shows that density functionals show efficient performance for gold-thiolate clusters. We can also use these results to generate large gold-thiolate nanoclusters. Scaling up the system requires sturdy knowledge of the use of proper theoretical methods. Our results provide a good description of the stable gold-thiolate structures and energetics. The detailed benchmark analysis vastly reinforces the use of GGA density functional PBE to obtain the most accurate geometries with an overall low computational cost. BP86 has the lower computational cost, is less accurate than PBE. Here, we have considered only the neutral ‘closed-shell’ systems to avoid spin contamination; hence, there is ample room for further studies with open-shell clusters. Besides, the benchmark study on relative energy ensure the overall stability of bridging Au-S-Au bonds over single-coordinated Au-S interaction and tri-coordinated Au₃-S interactions. We have seen that M06-2X outperforms other density functionals in predicting the relative stability of the minima. Although PBE0 and mPW1PW has consistent performance for both geometry optimization and relative stability calculation, at the same time, the computational cost is higher and can be used as a supporting method for further confirmation of the results. Double hybrid B2PLYP has also comparable performance with respect to RI-SCS-MP2 for stability study, however the range-separated hybrids and popular hybrid-GGA B3LYP are less promising in this pursuit.

With a $d^{10}s^1$ electronic configuration, gold atoms can form bonds with neighbouring atoms through both $6s$ and $5d$ valence orbitals. Au $6s$ orbital has one electron to interact with the other participating atoms. Likewise, interaction with a filled Au d orbital involves a pair of electrons from the Au atom. In between these two extremes, a variation of s - d mixing can lead to a continuum of coordination mode for Au and S in gold-thiolate nanoclusters. Therefore, it arises a complex bonding dependent on the extent of s - d hybridization for Au atoms. Our analysis shows that Au-S bond polarization is essential to generate bonding forces similar to Au-Au aurophilic interaction ('closed-shell' type interaction). So, the bonding is highly dependent on the extent of electronegativity-induced polarisation and hybridization of Au orbitals.¹⁹ From molecular AuSCH₃ to Au₃(SCH₃)₃ nanocluster, we have noticed a drop in covalency between Au and S atom due to higher repulsion energy as inferred from the Pauli repulsion. Greater s - d mixing in Au orbitals in cluster leads to a favorable polarisation effect. As a result, a higher charge transfer from Au to SCH₃ ligand is observed than that of an isolated AuSCH₃ molecule. Hence, we predict that the Au-S bond in gold-thiolate nanoclusters is a combination of several stabilizing factors. A charge-shift bond between Au and S thus gets stabilized mostly from ionic contribution. Further study on other energy-dependent parameters such as the free energy of gold-thiolate bond formation or dissociation should have a promising improvement over our current discussions.

Acknowledgement

We are thankful to Department of Science and Technology (DST), New Delhi, India for the FIST grants (SR/FST/CSII-026/2013 and SR/FST/CSII-011/2005). M K thanks DST for INSPIRE fellowship. S P and S R acknowledge IIT Kharagpur and S D shows gratitude to UGC for Financial support. We greatly acknowledge the resources of the Supercomputing facility at the Indian Institute of Technology Kharagpur established under National Supercomputing Mission (NSM), Government of India and supported by Centre for Development

of Advanced Computing (CDAC), Pune.

Supporting Information Available

References

- (1) Tiekink, E. R. Gold compounds in medicine: potential anti-tumour agents. *Gold Bulletin* **2003**, *36*, 117–124.
- (2) Ramanan, R.; Danovich, D.; Mandal, D.; Shaik, S. Catalysis of methyl transfer reactions by oriented external electric fields: Are gold–thiolate linkers innocent? *Journal of the American Chemical Society* **2018**, *140*, 4354–4362.
- (3) Hernández-Santos, D.; González-García, M. B.; García, A. C. Metal-nanoparticles based electroanalysis. *Electroanalysis: An International Journal Devoted to Fundamental and Practical Aspects of Electroanalysis* **2002**, *14*, 1225–1235.
- (4) Schaaff, T.; Shafigullin, M.; Khoury, J.; Vezmar, I.; Whetten, R.; Cullen, W.; First, P.; Gutierrez-Wing, C.; Ascensio, J.; Jose-Yacaman, M. Isolation of smaller nanocrystal Au molecules: robust quantum effects in optical spectra. *The Journal of Physical Chemistry B* **1997**, *101*, 7885–7891.
- (5) Qian, H.; Zhu, M.; Wu, Z.; Jin, R. Quantum sized gold nanoclusters with atomic precision. *Accounts of chemical research* **2012**, *45*, 1470–1479.
- (6) Blanc, J.; Bonačić-Koutecký, V.; Broyer, M.; Chevaleyre, J.; Dugourd, P.; Koutecký, J.; Scheuch, C.; Wolf, J.; Wöste, L. Evolution of the electronic structure of lithium clusters between four and eight atoms. *The Journal of chemical physics* **1992**, *96*, 1793–1809.
- (7) Pei, Y.; Zeng, X. C. Investigating the structural evolution of thiolate protected gold clusters from first-principles. *Nanoscale* **2012**, *4*, 4054–4072.

- (8) Maksymovych, P.; Sorescu, D. C.; Yates Jr, J. T. Gold-atom-mediated bonding in self-assembled short-chain alkanethiolate species on the Au (111) surface. *Physical review letters* **2006**, *97*, 146103.
- (9) Tian, Z.; Xu, Y.; Cheng, L. New Perspectives on the Electronic and Geometric Structure of Au₇₀S₂₀ (PPh₃)₁₂ Cluster: Superatomic-Network Core Protected by Novel Au₁₂(μ -S)₁₀ Staple Motifs. *Nanomaterials* **2019**, *9*, 1132.
- (10) Jadzinsky, P. D.; Calero, G.; Ackerson, C. J.; Bushnell, D. A.; Kornberg, R. D. Structure of a thiol monolayer-protected gold nanoparticle at 1.1 Å resolution. *science* **2007**, *318*, 430–433.
- (11) Daniel, M.-C.; Astruc, D. Gold nanoparticles: assembly, supramolecular chemistry, quantum-size-related properties, and applications toward biology, catalysis, and nanotechnology. *Chemical reviews* **2004**, *104*, 293–346.
- (12) Nobusada, K. Electronic structure and photochemical properties of a monolayer-protected gold cluster. *The Journal of Physical Chemistry B* **2004**, *108*, 11904–11908.
- (13) Häkkinen, H.; Walter, M.; Grönbeck, H. Divide and protect: capping gold nanoclusters with molecular gold-thiolate rings. *The Journal of Physical Chemistry B* **2006**, *110*, 9927–9931.
- (14) Jiang, D.-e.; Tiago, M. L.; Luo, W.; Dai, S. The “staple” motif: A key to stability of thiolate-protected gold nanoclusters. *Journal of the American Chemical Society* **2008**, *130*, 2777–2779.
- (15) Krüger, D.; Fuchs, H.; Rousseau, R.; Marx, D.; Parrinello, M. Interaction of short-chain alkane thiols and thiolates with small gold clusters: Adsorption structures and energetics. *The Journal of Chemical Physics* **2001**, *115*, 4776–4786.

- (16) Letardi, S.; Cleri, F. Interaction of benzene thiol and thiolate with small gold clusters. *The Journal of chemical physics* **2004**, *120*, 10062–10068.
- (17) Grönbeck, H.; Curioni, A.; Andreoni, W. Thiols and disulfides on the Au (111) surface: the headgroup- gold interaction. *Journal of the American Chemical Society* **2000**, *122*, 3839–3842.
- (18) Genest, A.; Krüger, S.; Gordienko, A. B.; Rösch, N. Gold-Thiolate Clusters: A Relativistic Density Functional Study of the Model Species Au₁₃ (SR)_n, R= H, CH₃, n= 4, 6, 8. *Zeitschrift für Naturforschung B* **2004**, *59*, 1585–1599.
- (19) Reimers, J. R.; Ford, M. J.; Halder, A.; Ulstrup, J.; Hush, N. S. Gold surfaces and nanoparticles are protected by Au (0)-thiyl species and are destroyed when Au (I)-thiolates form. *Proceedings of the National Academy of Sciences* **2016**, *113*, E1424–E1433.
- (20) Bader, R. F. W. *Atoms in Molecules: A Quantum Theory*. **1990**,
- (21) Wiberg, K. B. Application of the pople-santry-segal CNDO method to the cyclopropyl-carbinyl and cyclobutyl cation and to bicyclobutane. *Tetrahedron* **1968**, *24*, 1083–1096.
- (22) Mayer, I. Charge, bond order and valence in the AB initio SCF theory. *Chemical Physics Letters* **1983**, *97*, 270–274.
- (23) Reed, A. E.; Weinstock, R. B.; Weinhold, F. Natural population analysis. *The Journal of Chemical Physics* **1985**, *83*, 735–746.
- (24) Levine, D. S.; Head-Gordon, M. Quantifying the role of orbital contraction in chemical bonding. *The journal of physical chemistry letters* **2017**, *8*, 1967–1972.
- (25) Levine, D. S.; Head-Gordon, M. Energy decomposition analysis of single bonds within Kohn–Sham density functional theory. *Proceedings of the National Academy of Sciences* **2017**, *114*, 12649–12656.

- (26) Levine, D. S.; Horn, P. R.; Mao, Y.; Head-Gordon, M. Variational energy decomposition analysis of chemical bonding. 1. Spin-pure analysis of single bonds. *Journal of chemical theory and computation* **2016**, *12*, 4812–4820.
- (27) Grimme, S. Improved second-order Møller–Plesset perturbation theory by separate scaling of parallel- and antiparallel-spin pair correlation energies. *The Journal of chemical physics* **2003**, *118*, 9095–9102.
- (28) Grimme, S.; Antony, J.; Ehrlich, S.; Krieg, H. A consistent and accurate ab initio parametrization of density functional dispersion correction (DFT-D) for the 94 elements H–Pu. *The Journal of chemical physics* **2010**, *132*, 154104.
- (29) Grimme, S.; Ehrlich, S.; Goerigk, L. Effect of the damping function in dispersion corrected density functional theory. *Journal of computational chemistry* **2011**, *32*, 1456–1465.
- (30) Caldeweyher, E.; Mewes, J.-M.; Ehlert, S.; Grimme, S. Extension and evaluation of the D4 London-dispersion model for periodic systems. *Physical Chemistry Chemical Physics* **2020**, *22*, 8499–8512.
- (31) Becke, A. D. Density-functional exchange-energy approximation with correct asymptotic behavior. *Phys. Rev. A* **1988**, *38*, 3098–3100.
- (32) Perdew, J. P. Density-functional approximation for the correlation energy of the inhomogeneous electron gas. *Physical Review B* **1986**, *33*, 8822.
- (33) Zhao, Y.; Truhlar, D. G. A new local density functional for main-group thermochemistry, transition metal bonding, thermochemical kinetics, and noncovalent interactions. *The Journal of Chemical Physics* **2006**, *125*, 194101.
- (34) Zhao, Y.; Truhlar, D. G. The M06 suite of density functionals for main group thermochemistry, thermochemical kinetics, noncovalent interactions, excited states, and

- transition elements: two new functionals and systematic testing of four M06-class functionals and 12 other functionals. *Theoretical chemistry accounts* **2008**, *120*, 215–241.
- (35) Becke, A. D. Density-functional thermochemistry. I. The effect of the exchange-only gradient correction. *The Journal of chemical physics* **1992**, *96*, 2155–2160.
- (36) Lee, C.; Yang, W.; Parr, R. G. Development of the Colle-Salvetti correlation-energy formula into a functional of the electron density. *Physical review B* **1988**, *37*, 785.
- (37) Zhao, Y.; Truhlar, D. G. Design of density functionals that are broadly accurate for thermochemistry, thermochemical kinetics, and nonbonded interactions. *The Journal of Physical Chemistry A* **2005**, *109*, 5656–5667.
- (38) Chai, J.-D.; Head-Gordon, M. Systematic optimization of long-range corrected hybrid density functionals. *The Journal of Chemical Physics* **2008**, *128*, 084106.
- (39) Grimme, S. Semiempirical hybrid density functional with perturbative second-order correlation. *The Journal of chemical physics* **2006**, *124*, 034108.
- (40) Adamo, C.; Barone, V. Exchange functionals with improved long-range behavior and adiabatic connection methods without adjustable parameters: The mPW and mPW1PW models. *The Journal of Chemical Physics* **1998**, *108*, 664–675.
- (41) Perdew, J. P.; Chevary, J. A.; Vosko, S. H.; Jackson, K. A.; Pederson, M. R.; Singh, D. J.; Fiolhais, C. Atoms, molecules, solids, and surfaces: Applications of the generalized gradient approximation for exchange and correlation. *Phys. Rev. B* **1992**, *46*, 6671–6687.
- (42) Staroverov, V. N.; Scuseria, G. E.; Tao, J.; Perdew, J. P. Comparative assessment of a new nonempirical density functional: Molecules and hydrogen-bonded complexes. *The Journal of Chemical Physics* **2003**, *119*, 12129–12137.

- (43) Tao, J.; Perdew, J. P.; Staroverov, V. N.; Scuseria, G. E. Climbing the Density Functional Ladder: Nonempirical Meta-Generalized Gradient Approximation Designed for Molecules and Solids. *Phys. Rev. Lett.* **2003**, *91*, 146401.
- (44) Grimme, S. Density functional theory with London dispersion corrections. *Wiley Interdisciplinary Reviews: Computational Molecular Science* **2011**, *1*, 211–228.
- (45) Perdew, J. P.; Burke, K.; Ernzerhof, M. Generalized Gradient Approximation Made Simple. *Phys. Rev. Lett.* **1996**, *77*, 3865–3868.
- (46) Adamo, C.; Barone, V. Toward reliable density functional methods without adjustable parameters: The PBE0 model. *The Journal of chemical physics* **1999**, *110*, 6158–6170.
- (47) Zhang, Y.; Yang, W. Comment on “Generalized Gradient Approximation Made Simple”. *Phys. Rev. Lett.* **1998**, *80*, 890–890.
- (48) Riplinger, C.; Neese, F. An efficient and near linear scaling pair natural orbital based local coupled cluster method. *The Journal of chemical physics* **2013**, *138*, 034106.
- (49) Riplinger, C.; Sandhoefer, B.; Hansen, A.; Neese, F. Natural triple excitations in local coupled cluster calculations with pair natural orbitals. *The Journal of chemical physics* **2013**, *139*, 134101.
- (50) Neese, F. Software update: the ORCA program system, version 4.0. *Wiley Interdisciplinary Reviews: Computational Molecular Science* **2018**, *8*, e1327.
- (51) Weigend, F.; Ahlrichs, R. Balanced basis sets of split valence, triple zeta valence and quadruple zeta valence quality for H to Rn: Design and assessment of accuracy. *Physical Chemistry Chemical Physics* **2005**, *7*, 3297–3305.
- (52) Xu, X.; Truhlar, D. G. Accuracy of effective core potentials and basis sets for density functional calculations, including relativistic effects, as illustrated by calculations on arsenic compounds. *Journal of chemical theory and computation* **2011**, *7*, 2766–2779.

- (53) Kossmann, S.; Neese, F. Efficient structure optimization with second-order many-body perturbation theory: The RIJCOSX-MP2 method. *Journal of chemical theory and computation* **2010**, *6*, 2325–2338.
- (54) Lu, T.; Chen, F. Multiwfn: A Multifunctional Wavefunction Analyzer. *J. Comput. Chem.* **2012**, *33*, 580–592.
- (55) Frisch, M. J. et al. Gaussian 16 Revision B.01. 2016; Gaussian Inc. Wallingford CT.
- (56) Shao, Y. et al. Advances in molecular quantum chemistry contained in the Q-Chem 4 program package. *Molecular Physics* **2015**, *113*, 184–215.
- (57) Gilbert, A. IQmol, 2019.
- (58) Bau, R. Crystal structure of the antiarthritic drug gold thiomalate (myochrysin): a double-helical geometry in the solid state. *Journal of the American Chemical Society* **1998**, *120*, 9380–9381.
- (59) Negishi, Y.; Nobusada, K.; Tsukuda, T. Glutathione-protected gold clusters revisited: bridging the gap between gold (I)- thiolate complexes and thiolate-protected gold nanocrystals. *Journal of the American Chemical Society* **2005**, *127*, 5261–5270.
- (60) Shaw, C. F. Gold-based therapeutic agents. *Chemical reviews* **1999**, *99*, 2589–2600.
- (61) Bachman, R. E.; Bodolosky-Bettis, S. A.; Glennon, S. C.; Sirchio, S. A. Formation of a novel luminescent form of Gold (I) Phenylthiolate via self-assembly and decomposition of Isonitrilegold (I) Phenylthiolate Complexes. *Journal of the American Chemical Society* **2000**, *122*, 7146–7147.
- (62) Grönbeck, H.; Walter, M.; Häkkinen, H. Theoretical characterization of cyclic thiolated gold clusters. *Journal of the American Chemical Society* **2006**, *128*, 10268–10275.
- (63) Ge, S.; Zhao, J.; Ma, G. Thiol stabilized extremely small gold cluster complexes with high photoluminescence. *Inorganic Chemistry Communications* **2019**, *109*, 107556.

- (64) Häkkinen, H. The gold–sulfur interface at the nanoscale. *Nature chemistry* **2012**, *4*, 443.
- (65) Bürgi, T. Properties of the gold–sulphur interface: from self-assembled monolayers to clusters. *Nanoscale* **2015**, *7*, 15553–15567.
- (66) Hayashi, T.; Morikawa, Y.; Nozoye, H. Adsorption state of dimethyl disulfide on Au (111): Evidence for adsorption as thiolate at the bridge site. *The Journal of Chemical Physics* **2001**, *114*, 7615–7621.
- (67) Vargas, M. C.; Giannozzi, P.; Selloni, A.; Scoles, G. Coverage-dependent adsorption of CH₃S and (CH₃S)₂ on Au (111): A density functional theory study. *The Journal of Physical Chemistry B* **2001**, *105*, 9509–9513.
- (68) Gottschalck, J.; Hammer, B. A density functional theory study of the adsorption of sulfur, mercapto, and methylthiolate on Au (111). *The Journal of chemical physics* **2002**, *116*, 784–790.
- (69) Cremer, D.; Kraka, E. Chemical Bonds without Bonding Electron Density — Does the Difference Electron-Density Analysis Suffice for a Description of the Chemical Bond? *Angew. Chem., Int. Ed. Engl.* **1984**, *23*, 627–628.
- (70) Macchi, P.; Proserpio, D. M.; Sironi, A. Experimental Electron Density in a Transition Metal Dimer: Metal-Metal and Metal-Ligand Bonds. *J. Am. Chem. Soc.* **1998**, *120*, 13429–13435.
- (71) Macchi, P.; Garlaschelli, L.; Martinengo, S.; Sironi, A. Charge Density in Transition Metal Clusters: Supported vs Unsupported Metal-Metal Interactions. *J. Am. Chem. Soc.* **1999**, *121*, 10428–10429.
- (72) Novozhilova, I. V.; Volkov, A. V.; Coppens, P. Theoretical Analysis of the Triplet

- Excited State of the $[\text{Pt}_2(\text{H}_2\text{P}_2\text{O}_5)_4]^{4-}$ Ion and Comparison with Time-Resolved X-ray and Spectroscopic Results. *J. Am. Chem. Soc.* **2003**, *125*, 1079–1087.
- (73) Ziólkowski, M.; Grabowski, S. J.; Leszczynski, J. Cooperativity in Hydrogen-Bonded Interactions: Ab Initio and “Atoms in Molecules” Analyses. *J. Phys. Chem. A* **2006**, *110*, 6514–6521.
- (74) Horn, P. R.; Mao, Y.; Head-Gordon, M. Defining the contributions of permanent electrostatics, Pauli repulsion, and dispersion in density functional theory calculations of intermolecular interaction energies. *The Journal of chemical physics* **2016**, *144*, 114107.
- (75) Shaik, S.; Danovich, D.; Wu, W.; Hiberty, P. C. Charge-shift bonding and its manifestations in chemistry. *Nature chemistry* **2009**, *1*, 443–449.
- (76) Rahm, M.; Hoffmann, R. Distinguishing bonds. *Journal of the American Chemical Society* **2016**, *138*, 3731–3744.